A flexible luminescent probe to monitor fast ion losses at the edge of the TJ-II stellarator

D. Jiménez-Rey,[1,a] B. Zurro,[1] J. Guasp,[1] M. Liniers,[1] A. Baciero,[1] M. García-Muñoz,[2] A. Fernández,[1] G. García,[3] L. Rodríguez-Barquero,[4] and J. M. Fontdecaba[1]

[1]*Laboratorio Nacional de Fusión, Asociación Euratom-CIEMAT, Avda. Complutense 22, E-28040 Madrid, Spain*
[2]*Max-Planck-Institut für Plasmaphysik, EURATOM Association, Boltzmannstr. 2, Garching D-85748, Germany*
[3]*Instituto de Matemáticas y Física Fundamental, Consejo Superior de Investigaciones Científicas, Serrano 113-bis, 28006 Madrid, Spain*
[4]*Laboratorio de Metrología de Radiaciones Ionizantes, CIEMAT, Avda. Complutense 22, E-28040 Madrid, Spain*

A mobile luminescent probe has been developed to detect fast ion losses and suprathermal ions escaping from the plasma of the TJ-II stellarator device. The priorities for its design have been flexibility for probe positioning, ease of maintenance, and detector sensitivity. It employs a coherent fiber bundle to relay, to the outside of the vacuum chamber, ionoluminescence images produced by the ions that impinge, after entering the detector head through a pinhole aperture, onto a screen of luminescent material. Ionoluminescence light detection is accomplished by a charge-coupled device camera and by a photomultiplier, both of which are optically coupled to the in-vacuum fiber bundle head by means of a standard optical setup. A detailed description of the detector, and the first results obtained when operated close to the plasma edge, are reported. © *2008 American Institute of Physics.* [DOI: 10.1063/1.2979013]

I. INTRODUCTION

There exist several outstanding and fundamental issues related to the generation, confinement, and loss of fast ions, in particular, with regard to the standard methods used to heat fusion plasmas, i.e., radio frequency (rf) and neutral beam injection (NBI) heating, since thermal plasma particles are often heated by energetic ions. Therefore it is a primary challenge for experimentalists to estimate (or gather information on) the population of such ions and their distribution function, either with regard to their properties in the plasma interior or the loss component, since collisions with mechanical structure parts in the vacuum chamber could accelerate damage or contribute to plasma pollution by impurities. The behavior of fast ion confinement in medium sized stellarator devices can be benchmarked by using either the suprathermal ion population created by microwave heating[1,2] or by monitoring the nonthermalized fast ions associated with the NBI system.[3] Questions related to the dynamics of fast particles in driving magnetohydrodynamics (MHD) phenomena or in the generation of electric fields in plasmas constitute high-priority research efforts in plasma devices such as tokamaks and stellarators.[4,5] Fast ion confinement and loss mechanisms are controlled by effects associated with collisional transport, magnetic configuration peculiarities, heating method, and MHD activity originated by themselves or by other independent mechanisms.[6–9]

A new diagnostic, based on the ionoluminescence of a phosphor screen, has been installed in the TJ-II stellarator[10] for quantifying fast ion losses close to the plasma edge. This detector acts as a magnetic spectrometer where incident fast ions disperse, after passing through a pinhole aperture, onto a phosphor screen with a distribution that depends on ion gyroradius and pitch angle. The proper choice of detector geometry head with regard to the magnetic field structure impedes the passage of electrons onto the phosphor screen. Although this detector is based on principles similar to those of detectors operating in other plasma devices (Ref. 11, and references therein), the approach used here attempts to optimize the flexibility for diagnostic positioning and maintenance, as well as the sensitivity of light collection by using an original means to relay the phosphor screen luminescence to the detection components. Also, in contrast to other luminescence probes that are typically located close to the NBI injection port in order to collect the prompt ion losses, this system is located well away from the NBI injection ports and therefore optimization of its sensitivity is essential for its success.

Due to the high sensitivity of its design, the potential of this detector is not only to monitor direct fast ion losses originating from the NBI (a main goal in other fusion devices) but also to detect and study the energy distribution of the suprathermal ion population, with both temporal and particle phase space resolutions, which is present in the TJ-II, as well as in other devices, when the plasma is created and heated by rf techniques. It is the first time that suprathermal ions produced by electron cyclotron resonance heating
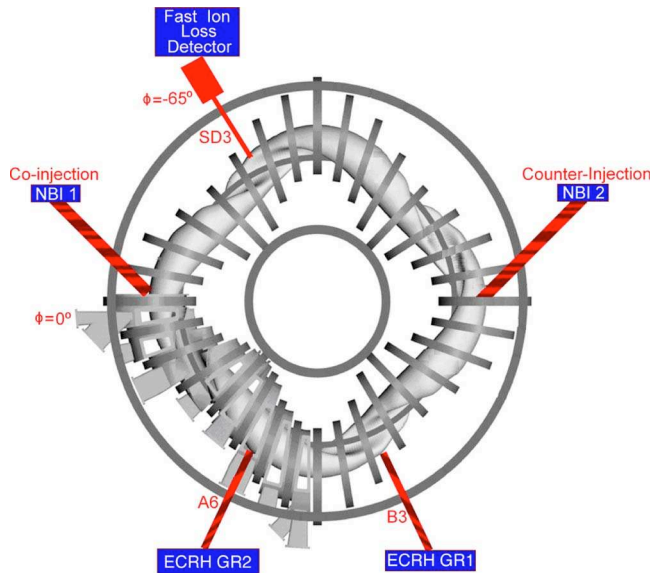

FIG. 1. (Color online) Top view of TJ-II device showing the locations of the magnetic field coils and the FILD with respect to the TJ-II heating systems.
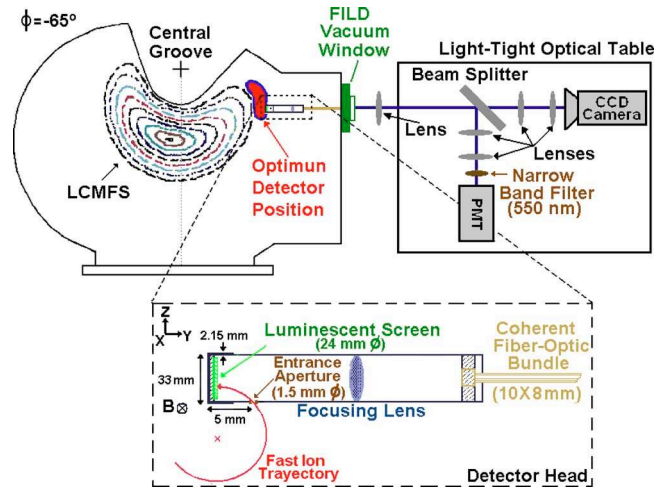

FIG. 2. (Color online) Sketches of the detector, the TJ-II vacuum chamber, and the TJ-II plasma shape. The LCMFS is indicated. An expanded view of the detector head is shown within the dashed rectangle.

(ECRH) are measured with a luminescent probe. This suprathermal population was detected previously in the TJ-II when its role in heating the thermal population was studied using spectroscopic techniques.[1] A detector of this kind can record ions that are difficult to measure using charge-exchange neutral spectrometers or classical spectroscopic diagnostics that view the plasma through perpendicular or tangential views, since such ions when drifting outside the plasma along paths not connected with exterior may not necessarily be seen by these more standard diagnostics. Moreover, a fast ion loss detector (FILD) detects ions directly without the need for these to be neutralized through charge-exchange processes.

The ultimate goal of this detector is to determine the energy and pitch angle distribution functions of ions impinging onto the phosphor screen so as to display such distributions on an absolute scale. To help calibrate the TJ-II measurements, a benchtop setup was developed in parallel to perform basic studies on the response of the phosphor screen in the ion energy range of interest ($E \leq 35$ keV).[12] In the past, the efficiency of phosphor screens to vacuum ultraviolet radiation, x rays and electrons has been studied extensively, but the response to ions in the energy range of interest for a FILD in fusion plasmas was unknown. This limitation has constrained the use of this type of detector to applications that did not require knowledge of the screen's ionoluminescent response with energy, for instance, the correlation of fast ions escaping with MHD plasma activity[3,9] or comparative measurements of ion impact position with ion energy. However, knowledge of luminescent material response with ion energy opens new avenues for the application of this type of detector.

This paper is organized as follows: first, a brief description of the system design and of its novel features and capabilities are presented. Second, the luminescent response of the screen used, measured in a laboratory setup, is presented.

Finally, the first results obtained in TJ-II plasma discharges are shown and discussed within the context of fast particle physics in stellarator devices.

II. DETECTOR DESCRIPTION

The operation principle is the detection of ionoluminescence from a granular luminescent screen. Such a phosphor screen was previously used in other such designs.[11] Indeed, it had been determined from measurements performed on a test bed[12] that this type of screen is more efficient than crystalline or ceramic ones within the specific energy range of this detector, i.e., ≤ 35 keV. The unique features of the design presented here include: (a) the flexibility to position the head due to the use of a coherent fiber optic bundle (8×10 mm^2 collection area and 90 cm long) that relays the ionoluminescent image from the plasma edge to outside of the vacuum chamber; (b) the possibility to orient the entrance aperture to sense ions coming from both toroidal directions and (c) its ease of extraction from the vacuum chamber for alignment, modification, or maintenance. In Fig. 1, the detector position is shown with respect to the TJ-II and its heating systems. In Fig. 2 a schematic representation of the FILD experimental setup is shown, and Fig. 3 illustrates the expected trajectories of ions relative to the phosphor screen.
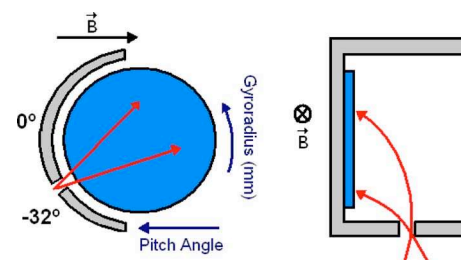

FIG. 3. (Color online) Schematic picture of its principle of operation showing how the ion impact point varies with gyroradius and pitch angle.
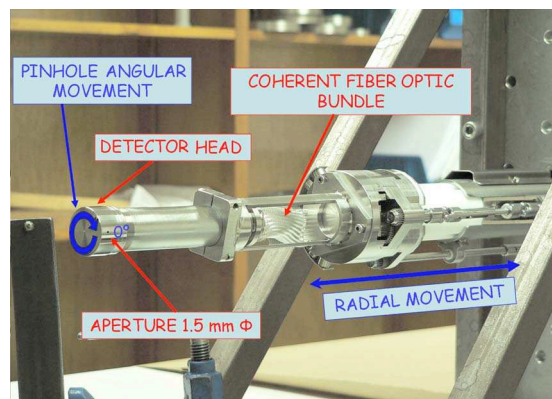
FIG. 4. (Color online) In the photograph of the detector prior to its installation in TJ-II, the red labels indicate the main detector components while the blue labels highlight the available movements.

A. Design constrains

The TJ-II device[10] is a four-period, low magnetic shear, stellarator with a major radius of 1.5 m and an average minor radius of ≤ 0.22 m. At present, central electron densities and temperatures up to 1.7×10^{19} m^{-3} and 2 keV, respectively, are achieved in plasmas created and maintained by ECRH using a frequency of 53.2 GHz tuned to the second harmonic, $P_{ecrh} \leq 600$ kW. Additional heating is available from two NBIs that are operated in co- and counterinjection. At present, each NBI injector produces ≤ 300 ms long pulses of neutral hydrogen accelerated to 31 keV (nominal energy mix ratio of 80:10:10) to provide <1 MW of nominal heating. Fast ion losses are predicted to play an important role in high density, and high beta NBI heated plasmas in this high ripple device. The TJ-II has been operated during the measurements reported here with a maximum ECR power of 600 kW, and in a few discharges with a coinjected NBI beam providing an absorbed power of 400–450 kW.

The conceptual design, the toroidal and poloidal location of the detector, as well as the peculiarities and complicated geometry of TJ-II, were outlined in more detail in a previous publication.[13] Since then some geometrical modifications have been made to the detector head. See Fig. 2, where dimensional details are provided. Next, we summarize the basic results needed to follow the argument of this paper. First, simulations made with the numerical Monte Carlo code, FAFNER 2,[13–15] predict that fast ion losses may reach up to 30% of the input power for the NBI parallel to the toroidal field (coinjection), and ~8% for the antiparallel NBI. Moreover, predictions suggest that such losses are dominated by direct losses, up to 80% of which go to the inaccessible central groove (see Fig. 2) of the TJ-II where they are extremely localized in the poloidal plane. Such localization has made diagnostic positioning flexibility an important design criterion and has been the motivation for achieving a high sensitivity design that is compatible with the TJ-II geometrical constrains. Second, the design avoids long fibers for relaying the luminescence light to detectors located outside the vacuum chamber. Rather, it incorporates a direct and compact optical coupling that is installed close (1–2 m) to the optical window where the exit end of the in-vacuum coherent fiber bundle is situated. Such a close placement is possible in

TJ-II because of the lack of hard radiation (i.e., gammas or neutrons).

B. Mechanical and vacuum designs

The photograph in Fig. 4 shows the detector head, with some of the parts, schematically shown in Fig. 2, identified. The core of the fast ion detector, i.e., the detector head and coherent bundle, is mounted on a movable shaft so that it can be inserted into and withdrawn from the TJ-II vacuum chamber. A stainless steel bellows allows a radial displacement of up to 460 mm, thereby permitting it to be displaced from its venting position, where the detector can be manipulated for alignment, calibration, and/or maintenance, to its working position close to the plasma edge. When the detector is located in the maintenance position, a manual gate valve isolates it the TJ-II chamber from the rest of the system so that it can be vented to air. To achieve the required radial scan capability, the entire system is supported by, and guided along, three rails that are fixed to the large access vacuum flange (247×537 mm^2) located in the sector. In addition, a quartz window (for light transmission), as well as an electrical feedthrough, are located on the flange.

C. Luminescence screen

The phosphor powder screen used, P45 ($Y_2O_2S:Tb$), was prepared in-house from commercially available phosphor grains, provided by Osram Sylvania (Towanda, USA). A uniform screen, deposited on a 25 mm diameter stainless steel plate, was prepared using a sedimentation method, explained in more detail in Ref. 12, to obtain a screen density of approximately 17.59 mg cm^{-2}. The luminescent centers are Tb^{+3} ions uniformly distributed in the Y_2O_2S host lattice. The main properties of this powder are a decay time of 1.4 ms, a main emission peak at 530 nm, and a low degradation of ionoluminescent efficiency with irradiation.[12]

This phosphor was chosen for this first phase of operation because of its good sensitivity and linearity in the energy range of interest for ion induced luminescence.[12] Previously, similar phosphor screens had been studied in a laboratory setup using a commercial ion source where they were bombarded by different ions (H$^+$, He$^+$, and Ar$^+$) with energies in the same range as those expected in TJ-II plasmas, i.e., up to 35 keV.[12] In this laboratory setup ionoluminescence, cathodoluminescence, and photoluminescence could be alternatively studied, thereby providing an excellent benchmark to study the influence of the different mechanisms and to obtain luminescent spectra at different ion energies.[12,16] Such measurements are essential when designing a phosphor screen-based detector (e.g., fast ion detector, soft x-ray detector, etc.). In Fig. 5 the ionoluminescence response of the P45 phosphor screen is depicted as a function of ion energy for two types of ions, H$^+$ and He$^+$; while in Fig. 6 broadband luminescence spectra, between 200 and 900 nm, are shown for H$^+$ ion energies up to 60 keV.

D. Optics

The detector optics is composed of two separate parts, one inside the vacuum chamber (inner optics) and located at
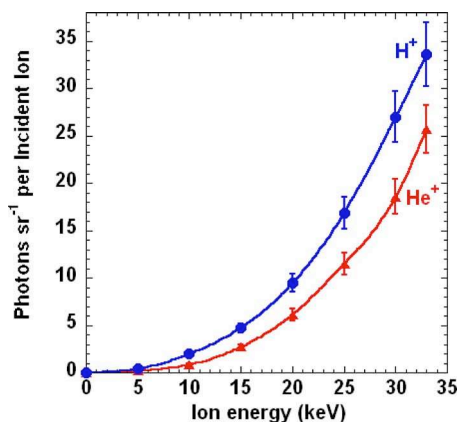
FIG. 5. (Color online) Ionoluminescent response of P45 to H^+ and He^+ ions, as measured in the laboratory setup, for ion acceleration energies up to the energies of the TJ-II neutral beam injectors (≤ 35 keV).
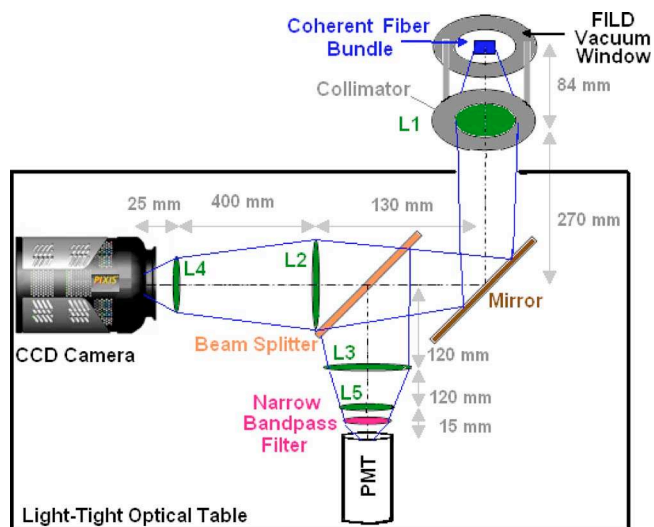

FIG. 7. (Color online) A schematic layout of collection and relay optics including detector positions. The entire system is enclosed on an in-house made, light-tight, optical table.

the head of the movable probe, see Fig. 2 and an external optics, which is sketched in Fig. 7. The external optics is located on a light-shielded optical table situated close to, but outside, the vacuum chamber. It is optically coupled to the exit end of the in-vacuum fiber optic bundle. A radial displacement of the probe also requires a displacement of the optical table. The optical components inside the TJ-II vacuum chamber include the luminescence screen (diameter of 25.4 mm), a lens (diameter of 25.6 mm, focal length of 33 mm), and the coherent fiber bundle. The coherent fiber bundle has an 8×10 mm^2 collection area and is 90 cm long (by Colutron Research, Boulder, USA). Next, a lens mounted on the outside of the vacuum flange transmission window collimates the light emerging from the fiber bundle exit end and guides it to the optical table, where the light detectors are located. There, the first component encountered by the light incident on the optical table is an aluminized mirror (100×100 mm^2) positioned on a high precision angular adjustable platform. It directs the collimated light toward a pellicle beam splitter (model 03BPL 011/04, Melles Griot, Holland) where part of the light is directed to a high sensitivity charge-coupled device (CCD) camera. The remaining 40% of the luminescence light is diverted to a second arm equipped with a photomultiplier tube (PMT) that detects the

FIG. 6. (Color online) P45 luminescent spectrum, between 200 and 900 nm, excited by H^+ ions up to 60 keV. A 2D spectrum is shown in the top right-hand corner.

light from across the whole luminescent screen. In addition, two lenses are located between the beam splitter and each detector, one of which serves to match the output fiber size to the detector sensitive area, while the second acts as a field lens for maximizing light collection. Finally, a narrow bandpass filter, centered at 530 nm, is placed in front of the PMT photocathode in order to pass the luminescence light while rejecting any background light coming from the plasma. Finally, by inserting the detector head inside the TJ-II vacuum chamber when performing glow discharge cleaning with helium, a very high light rejection capability was demonstrated, i.e., no light signal was detected.

E. Light detection

For the initial experimental phase, the luminescent light was guided to the PMT so as to obtain a continuous time response of the ionoluminescence system to plasma ions. The PMT is a compact model (H5784-04 by Hamamatsu) and its output is connected to a current amplifier (model 570 by Stanford Research Systems, Sunnyvale, CA, USA), with a bandwidth of 200 kHz for a standard gain of 1 μA/V. Simultaneously, the luminescent image of ion impacts on the luminescence screen was relayed to the cooled CCD camera to obtain energy and pitch angle resolution information. The camera selected for this is a back-illuminated CCD (2048 $\times$ 512 pixels) with a 13×13 μm^2 pixel size, model PIXIS 2KB by Princeton Instruments (Princeton, NJ, USA). The camera, working with an electromechanical shutter is operated in single shot mode with a preprogramed pulse time within the TJ-II discharge. Note the minimum aperture time of the mechanical shutter is 10 ms. In order to reduce this time window for applications demanding a shorter aperture time there exists the possibility of using a liquid crystal electro-optic shutter that can achieve exposure times of $100-200$ μs, (assuming that the signal levels are high enough).

Both data described above are needed to confirm that luminescence signals arise from ions impinging onto the
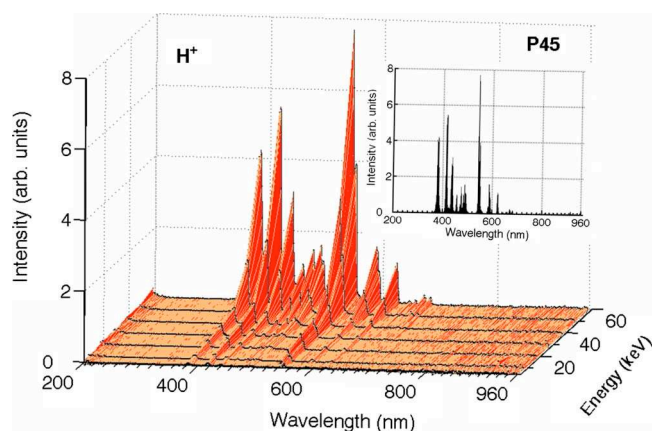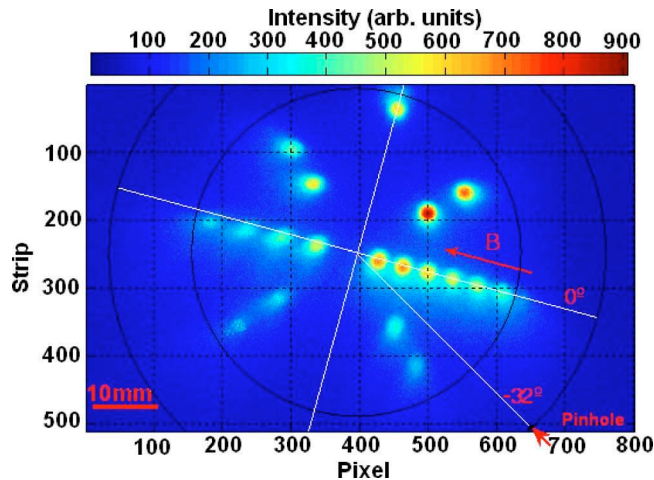
FIG. 8. (Color online) A CCD image obtained during the alignment and calibration process performed prior to installation in the TJ-II. For this purpose the phosphor screen is replaced by a black screen with a set of structured apertures/holes illuminated from behind by a uniform flat electroluminescent lamp. Different numbers of fiducial holes are used on the left and the right side of this calibration screen. Here, the full circle represents the phosphor screen size while the larger, partial circle is the metallic head.

phosphor screen, after passing through the 1.5 mm diameter collimating hole located in the head of the movable optical probe, rather than from other types of phosphor exciting agents; note that the phosphor screen can, in principle, respond to photons, electrons and ions (with $E \geq 1$ keV). Indeed an analysis of the temporal behavior of the ion detector signature, for different types of plasma discharges together with its correlation with time traces from radiation diagnostics covering different spectral ranges, e.g., visible, vuv and x rays, excluded other sources as contributing to the signal delivered to the photomultiplier detector. The latter point should be emphasized, since in contrast to other devices, this detector exhibits a significant response to ions ($E \geq 1$ keV) generated by ECRH, illustrating the high sensitivity of the present design.

F. Alignment and calibration

Optical alignment is checked in two separate steps prior to inserting the detector head into the vacuum chamber. First, the detector head is aligned to ensure that the coherent fiber bundle collects all the luminescence light emerging from the phosphor screen. Second, the opposite end of the fiber bundle is aligned with the collection/guiding optics and the light detectors. The first step is performed by illuminating the fiber bundle with a flashlight in order to fine-tune the detector head lens position and the orientation of the bundle so as to completely fill the phosphor screen with light. The second step consists of substituting the detector head tip containing the phosphor screen (it can be screwed off) with one incorporating a black screen of the same size. The black screen is structured with apertures/holes that are illuminated from behind by thin flat uniform electroluminescent lamp. Thus, by recording images with the camera the light path can be determined. See Fig. 8 where an image of the illuminated black screen recorded by the CCD camera is shown. This setup permits optimization of the focus while also allowing flat-

field calibration of the CCD images relative to the phosphor screen plane so that any variation in sensitivity or resolution across the luminescent screen can be included in the corresponding calibration factors.

Once installed inside the TJ-II vacuum chamber, two procedures are performed for routine alignment and stability checking. The first procedure involves attaching a flat electroluminescent lamp, with a mask for simulating the output face of the fiber bundle, to the outside of the vacuum window. The beam path inside the optical table is followed and position adjustments can be made. This visual alignment phase is followed by a finer alignment where the CCD camera and the PMT positions are fine-tuned in order to center the image on the CCD and to maximize the signal reaching the PMT. A less intrusive, but not so precise method is to illuminate the fiber bundle detector head with a flashlight through optical windows located in the same toroidal sector of the TJ-II as the detector itself. The screen is sufficiently well illuminated by this method so that the image of the scattered light in the phosphor or the entrance pinhole can be seen in the CCD camera, without any filter. Finally, the detector head is mechanically aligned close to the last closed magnetic field surface (LCMFS) using machine drawings and magnetic configuration maps. As TJ-II can be operated without current it was reasonable to assume that vacuum and real magnetic configurations concur.[10]

Hence, the alignment procedures described here, together with the response of phosphor screen as a function of ion energy, give calibrated data that can be compared to future theoretical simulations.

III. INITIAL RESULTS

The detector has been operated during this first phase in hydrogen discharges heated with ECRH alone as well as ECRH plus coinjection NBI. During this phase the detector response was checked at different radial positions, pinhole angles, and under different plasma conditions in order to highlight the geometrical flexibility of the FILD. For example, it has been operated at different distances from the plasma edge and with two different pinhole angles: (1) at 0° with respect to the toroidal magnetic field, where the detector axis is the diameter passing through the pinhole; and (2) at the theoretically optimum orientation of −32° suggested by previous numerical simulations,[13] in order to optimize the collection of fast ions originating from the NBI coinjector. The detector results obtained were then analyzed for the different conditions. In Sec. III A and III B the luminescence probe performance is illustrated by a selection of results, i.e., temporal PMT traces and CCD images, from different TJ-II plasma discharges.

A. PMT

A notable aspect of the results obtained in ECRH plasmas is the high signal level obtained. This would indicate that it should be possible to study the generation of ion tails, associated with ECRH and other rf heating schemes, a theme that has received attention recently in stellarator plasmas, see Refs. 1 and 2, and references therein. The detector response
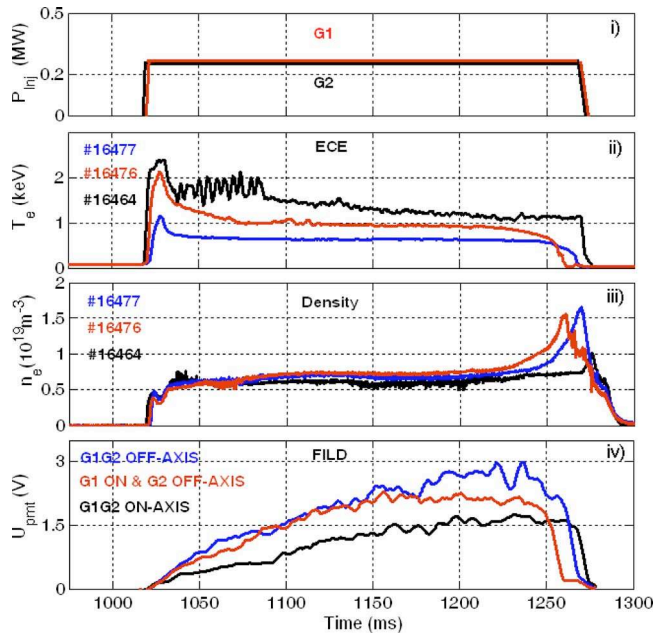
FIG. 9. (Color online) Signal traces for three similar ECRH heated discharges, (i) created with the same total injected power of 600 kW and for the same magnetic configuration, but with different power deposition profiles [see legends in (iv)]. Traces corresponding to electron temperature [from electron cyclotron emission (ECE) measurements] and line averaged densities are shown in (ii) and (iii), respectively. (iv) The FILD PMT response.

in such discharges is illustrated by the FILD signal traces plotted in Figs. 9 and 10. In Fig. 9 representative traces from the fast ion PMT detector are plotted for discharges with on- and off-axis deposition of the ECRH power. The signal levels monitored by the PMT are compared for tree cases: both gyrotrons on-axis (discharge No. 16464), both off-axis (discharge No. 16477), and an intermediate case with one gyrotron off axis and the other on-axis (discharge No. 16476). It
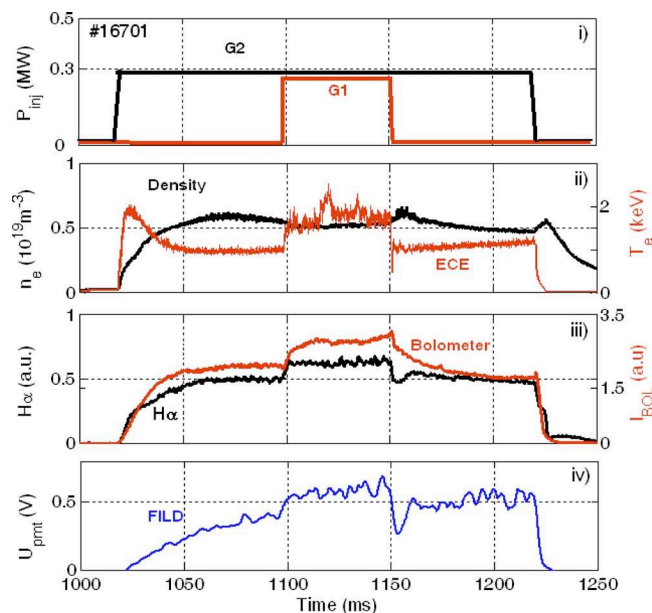

FIG. 10. (Color online) Signal traces for a discharge, sustained by gyrotron G2, where a 50 ms pulse of gyrotron G1 was applied during the discharge. Signal traces of (ii) ECE temperature and line averaged densities, (iii) total radiation and Hα emission, and (iv) FILD PMT are also shown.
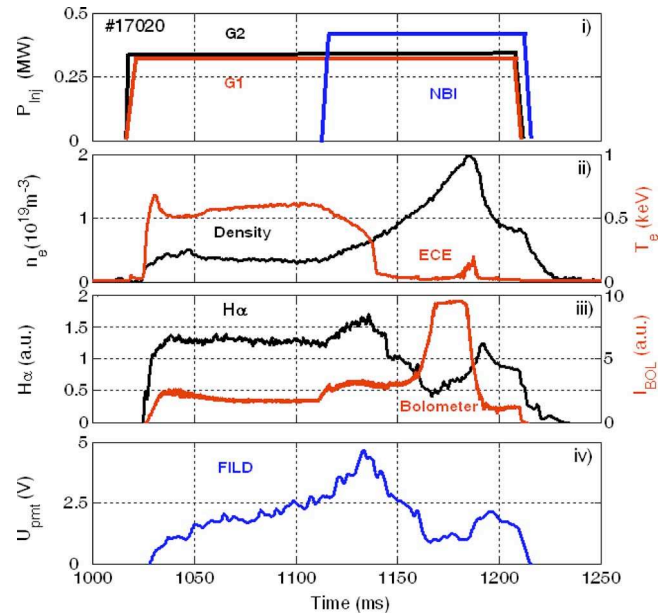

FIG. 11. (Color online) The FILD PMT response of an ECRH discharge, followed by a coinjection NBI pulse, for 0° angles of the collimation hole (No. 17020).

should be noted that for the detector head setup used here (detector pinhole at 0°), the maximum signal was achieved when both gyrotrons were off axis.

Next, in Fig. 10, the global response of the detector is depicted for an ECRH discharge created and maintained by a single gyrotron, with the second gyrotron delivering a 50 ms pulse in the middle of the discharge. It can be observed in the traces that the FILD responds to the microwave injected power. This is interpreted as arising from the generation of ions with energies ≥ 1 keV (the threshold value for phosphor screen response to protons). The fast rise in signal with the microwave heating perturbation precludes that it is due to a rise in radiation which has a different behavior or signature. It is hypothesized that these ions correspond to the suprathermal population associated with ECRH heating that was identified in a previous study performed in TJ-II using spectroscopy.[1]

In order to illustrate the flexibility of the detector as well as its sensitivity and dynamic range, some examples of the detector signature are shown in Figs. 11 and 12 for a plasma discharge created with ECRH and having a coinjection pulse of NBI heating. Here, plots are shown for two positions of the ion entrance pinhole, i.e., for 0° (Fig. 11, No. 17020,) and −32° (Fig. 12, No. 17844). In both cases a significant level of signal is observed during the ECRH phase, regardless of the pinhole angle, suggesting that the ECRH suprathermal ion tail causing this effect has a wide range of velocity directions. However, when recording fast ion losses during NBI injection, the aperture position becomes more critical, as was predicted by previous simulations.[12] This can be appreciated in Fig. 11 where the pinhole was oriented at 0°. Here, a small initial rise in the signal at the very beginning of the NBI phase is followed by a drop-off in detector response during the density rise phase of the NBI injection. It can be concluded that no signature is left by the fast ion loss compo-
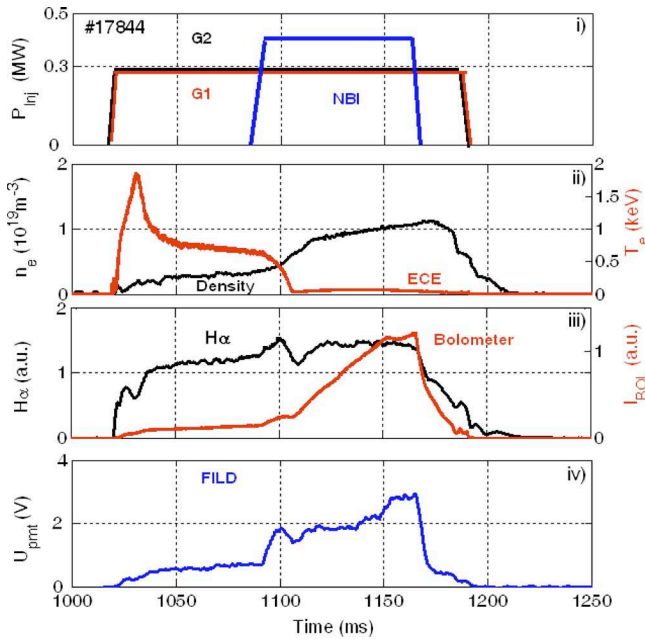
FIG. 12. (Color online) The FILD PMT response of an ECRH discharge, followed by a coinjection NBI pulse, for −32° angles of the collimation hole (No. 17844). Signal coming from the NBI is seen only for the −32° case.

nents associated with NBI injection while a reduction in the fast ion tail, associated with ECRH, is observed due in part to the cutoff of the heating microwaves that results when the plasma electron density rises above cutoff, i.e., $>1.7 \times 10^{19}$ m^{-3}. However, in Fig. 12, where the pinhole angle is set to approximately −32°,[11] a significant increase in signal level, with respect to that during the ECRH phase (by a factor of 2–4), is observed so this signature can be associated with the fast ion losses during the NBI injection phase.

B. CCD camera

An example of the results obtained with the CCD camera when imaging the phosphor screen during the NBI phase is shown in Fig. 13 together with PMT signal evolution traces (Fig. 14). In Fig. 13, the image presented is from a discharge (No. 17954) during which the neutral beam is injected into a low temperature plasma. For this the CCD image was integrated for 50 ms during the NBI phase, starting at 1100 ms. See Fig. 14 where signal traces from other plasma diagnostics are shown. Now, the tracks created on the phosphor screen by the ions escaping from the plasma are seen in the recorded image. It should be noted that this is a good procedure for checking *in situ* the energy mapping of the detector. The three strips with different intensities seen in the two dimensional (2D) image correspond to the three energy components of the beam, i.e., E, $E/2$, and $E/3$, where E represents the accelerating energy of the H neutrals. Here, for this case these are seen to be almost unaffected by the cold plasma. Next, image intensities along several horizontal lines of the same CCD image are also provided. In these cases the intermediate energy component, $E/2$, appears as the most intense one. This is because the main energy component (30 keV) suffers from significant shine through losses in low temperature discharges and therefore fewer ions of
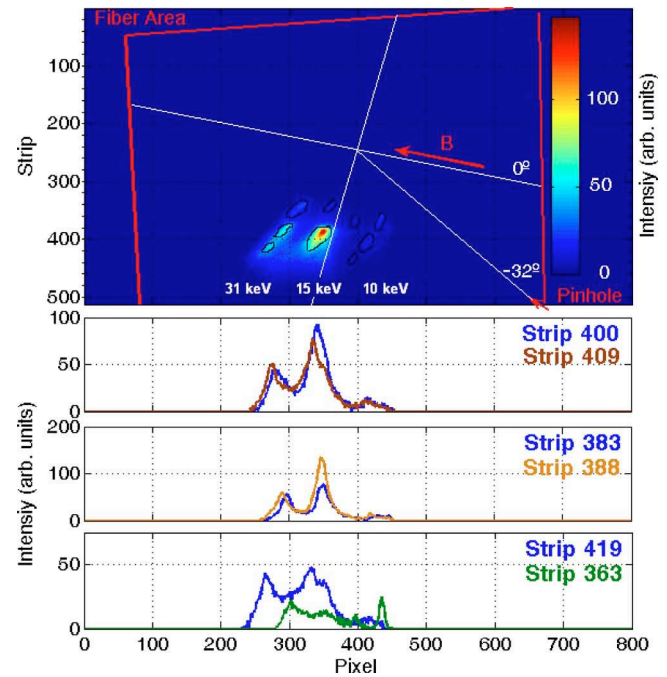

FIG. 13. (Color online) Detector results from a discharge (No. 17954) where NBI was injected during the cold plasma phase. A FILD screen image highlighting ion strikes created by the three energy components of the NBI as a result of its poor interaction with the cold plasma. Note that the red rectangle corresponds to the fiber bundle. The pinhole position and magnetic field direction are also shown. Below the image, signal intensities along three different horizontal lines are plotted to emphasize the beam components.

that energy can reach the toroidal sector where the ionoluminescence detector is located. See Figs. 1 and 2.

In Fig. 15, a comparison is made between the tracks left on the phosphor screen by ions in two different discharges.
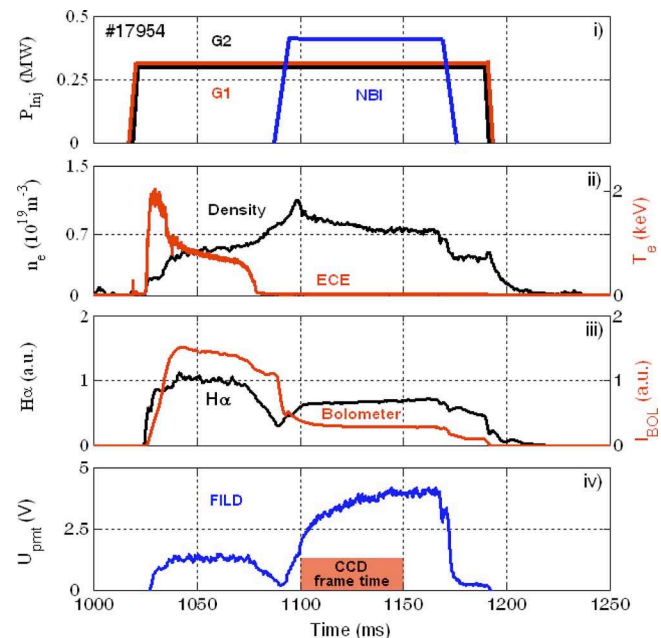

FIG. 14. (Color online) Signal traces from the discharge (No. 17954) where NBI was injected during the cold plasma phase showing the (i) heating pulses, (ii) ECE temperature and line averaged densities, (iii) total radiation and Hα emission, and (iv) FILD PMT.
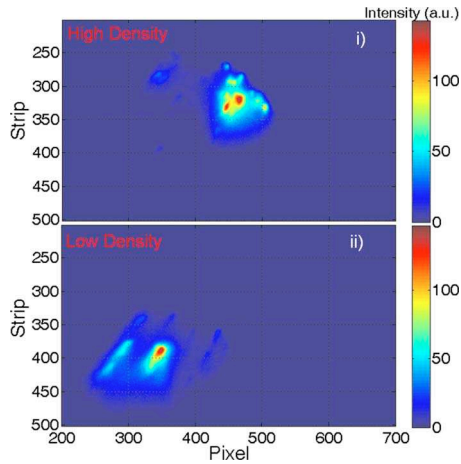
FIG. 15. (Color online) Comparison of the screen image obtained for the cold discharge of Fig. 13 [bottom, (ii)], with that obtained during a typical NBI discharge [top, (i)] in order to highlight the differences in the positions of the tracks left by the NBI ions reaching the luminescent screen as consequence of the energy absorption and interaction in the plasma.

In the lower CCD image obtained in a low temperature plasma discharge, No. 17954, due exclusively to the fast ions coming directly from the NBI, after a modest interaction with the plasma. In the upper image, the tracks produced during a standard TJ-II discharge, (No. 17941), whose typical traces are shown in Fig. 16. Significant differences in the impact regions of the fast ions, associated with the slowing-down spectra of the full energy component, are clearly seen. Note that, in order to create this image, it was necessary to subtract the ECRH contribution. This was performed using the traces obtained for a similar TJ-II discharge without NBI heating.

The actual aperture, with the pinhole oriented at $-32°$ with respect to the local magnetic field, allows particles with pitch angles from approximately $20°$ to $80°$, cogoing, to be
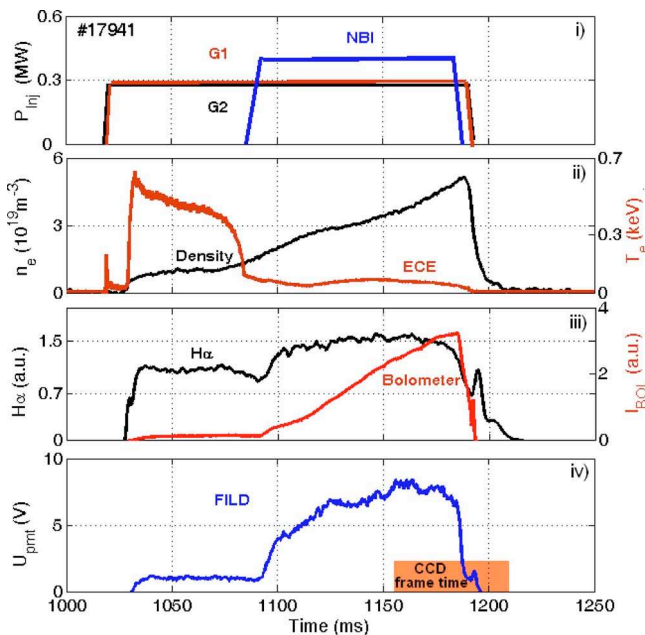

FIG. 16. (Color online) Standard traces of the hot discharge (No. 17941 high density discharge of Fig. 15).
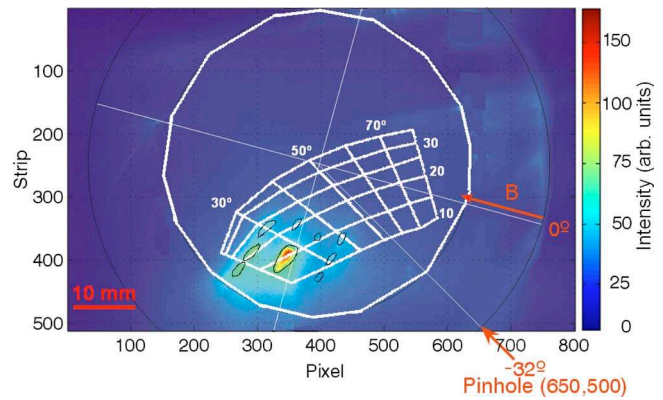

FIG. 17. (Color online) Superposition of the simulated grid for the geometry and magnetic field of the detector on the screen image obtained from discharge No. 17954 (cold discharge of Fig. 13).

detected. Finally, in Fig. 17 we superimpose the ion image obtained in the cold discharge (with $n_e \approx 7.5 \times 10^{18}$ m^{-3}) of Figs. 13 and 15 (ii) with the energy and pitch angle grid calculated using the Monte Carlo code.[8,9] This grid can be applied for all CCD images. The CCD data in Fig. 17, recorded during 50 ms [with $t(0) = 1100$ ms], exhibit loss distributions well localized in several different small areas, i.e., the main fast ion loss distribution in this discharge has a centroid at $27°$ (pitch angle) and 15 mm (gyroradius), for a magnetic field at the probe position up to 0.62 T. This most intense part corresponds to direct losses produced by means of NBI heating.

With in summary, fast ion losses were detected by means of a scintillator probe for the first time in TJ-II (2007). Losses were observed to be associated with NBI and with ECRH. It should be noted that both the PMT and CCD data have excellent signal to noise ratios. Finally, the system resolution has permitted discrimination between the full, half, and third energy components of the beam.

ACKNOWLEDGMENTS

[1] D. Rapisarda, B. Zurro, V. Tribaldos, A. Baciero, and TJ-II Team, Plasma Phys. Controlled Fusion **49**, 309 (2007).
[2] H. Okada, Y. Torii, S. Kobayashi, M. Kaneko, H. Kitagawa, T. Tomokiyo, H. Takahashi, T. Mutoh, T. Mizuuchi, K. Nagasaki, Y. Nakamura, S. Yamamoto, H. Arimoto, K. Hanatani, K. Kondo, and F. Sano, Nucl. Fusion **47**, 1346 (2007).
[3] D. Buchenauer, W. W. Heidbrink, L. Roquemore, and K. McGuire, Rev. Sci. Instrum. **58**, 2264 (1987).
[4] K. Shinohara, M. Isobe, and D. S. Darrow, Rev. Sci. Instrum. **77**, 10E521 (2006).
[5] T. Kondo, M. Isobe, M. Sasao, D. S. Darrow, K. Toi, M. Takechi, M. Osakabe, Y. Yoshimura, C. Takahashi, S. Nishimura, G. Matsunaga, S. Okamura, K. Matsuoka, and CHS Group, Nucl. Fusion **40**, 1575 (2000).
[6] K. Toi, M. Takechi, M. Isobe, N. Nakajima, M. Osakabe, S. Takagi, T. Kondo, G. Matsunaga, K. Ohkuni, M. Sasao, S. Yamamoto, S. Ohdachi, S. Sakakibara, H. Yamada, K.Y. Watanabe, D.S. Darrow, A. Fujisawa, M. Goto, K. Ida, H. Idei, H. Iguchi, S. Lee, S. Kado, S. Kubo, O. Kaneko, K. Kawahata, K. Matsuoka, T. Minami, S. Morita, O. Motojima, K. Narihara, S. Nishimura, N. Ohyabu, Y. Oka, S. Okamura, T. Ozaki, K. Sato, M.

Sato, A. Shimizu, T. Shimozuma, Y. Takeiri, K. Tanaka, T. Tokuzawa, K. Tsumori, I. Yamada, Y. Yoshimura, and CHS and LHD Experimental Groups, Nucl. Fusion **40**, 1349 (2000).

[7] K. G. McClements and A. Thyagaraja, Phys. Plasmas **13**, 042503 (2006).

[8] M. García-Muñoz, P. Martin, H.-U. Fahrbach, M. Gobbin, S. Günter, M. Maraschek, L. Marrelli, and H. Zohm, Nucl. Fusion **47**, L10 (2007).

[9] M. García-Munoz, H.-U. Fahrbach, S. Günter, V. Igochine, M. J. Mantsinen, M. Maraschek, P. Martin, P. Piovesan, K. Sassenberg, and H. Zohm, Phys. Rev. Lett. **100**, 055005 (2008).

[10] C. Alejaldre, J. Alonso, L. Almoguera, E. Ascasíbar, A. Baciero, R. Balbín, M. Blaumoser, J. Botija, B. Brañas, E. de la Cal, A. Cappa, R. Carrasco, F. Castejón, J. R. Cepero, C. Cremy, J. Doncel, C. Dulya, T. Estrada, A. Fernández, M. Francés, C. Fuentes, A. García, I. García-Cortés, J. Guasp, J. Herranz, C. Hidalgo, J. A. Jiménez, I. Kirpitchev, V. Krivenski, I. Labrador, F. Lapayese, K. Likin, M. Liniers, A. López-Fraguas, A. López-Sánchez, E. de la Luna, R. Martín, A. Martínez, M. Medrano, P. Méndez, K. McCarthy, F. Medina, B. van Milligen, M. Ochando, L. Pacios, I. Pastor, M. A. Pedrosa, A. de la Peña, A. Portas, J.

Qin, L. Rodríguez-Rodrigo, A. Salas, E. Sánchez, J. Sánchez, F. Tabarés, D. Tafalla, V. Tribaldos, J. Vega, B. Zurro, D. Akulina, O. I. Fedyanin, S. Grebenshchicov, N. Kharchev, A. Meshcheryakov, R. Barth, G. van Dijk, H. van der Meiden, and S. Petrov, Plasma Phys. Controlled Fusion **41**, A539 (1999).

[11] D. S. Darrow, Rev. Sci. Instrum. **79**, 023502 (2008).

[12] D. Jiménez-Rey, B. Zurro, G. García, A. Baciero, L. Rodríguez-Barquero, and M. García-Munoz, "Ionoluminescent response of several phosphor screens to keV ions of different masses," J. Appl. Phys. (to be published).

[13] C. Burgos, B. Zurro, J. Guasp, M. A. Ochando, K. J. McCarthy, F. Medina, A. Baciero, M. Liniers, and C. Fuentes, Rev. Sci. Instrum. **74**, 1861 (2003).

[14] J. Guasp, M. Liniers, C. Fuentes, and G. Barrera, Fusion Technol. **35**, 32 (1999).

[15] J. Guasp and M. Liniers, Fusion Technol. **34**, 251 (1993).

[16] D. Jiménez-Rey, B. Zurro, K. J. McCarthy, G. García, and A. Baciero, Rev. Sci. Instrum. (to be published).